

An improved particle packing algorithm for complex geometries in SPH

Pawan Negi^{a,*}, Prabhu Ramachandran^a

^a*Department of Aerospace Engineering, Indian Institute of Technology Bombay, Powai, Mumbai 400076*

Abstract

Accurate simulation of fluid flow in the presence of complex geometries with mesh-free methods requires that the geometry surfaces be captured accurately with particles. The traditional ways to do this with particles do not result in an accurate representation of the geometry surfaces. In this paper we propose a simple SPH-based algorithm to produce homogeneous particle distributions that capture the geometry surfaces accurately in two and three dimensions. Several benchmark problems are solved to demonstrate the accuracy of the new algorithm. The algorithm is open source and our manuscript is fully reproducible.

Keywords: Particle packing, complex geometry, pre-processing, smoothed particle hydrodynamics

1. Introduction

Smoothed Particle Hydrodynamics (SPH) is a mesh-free numerical method for simulation of continuum mechanics problems. It was first proposed by Gingold and Monaghan [1] and Lucy [2]. Unlike mesh-based methods, the SPH method employs particles that carry physical properties. The SPH method has been employed to study a wide variety of problems. In order to simulate problems involving complex shapes, we need to capture the important features of the geometry accurately. The particles must therefore be

*Corresponding author

Email addresses: `pawan.n@aero.iitb.ac.in` (Pawan Negi),
`prabhu@aero.iitb.ac.in` (Prabhu Ramachandran)

arranged carefully to capture the geometry and must also be homogeneous for the SPH method to be accurate and effective. There have been some earlier attempts to do this in the context of SPH in [3, 4, 5].

Colagrossi et al. [5], proposes a particle packing algorithm which uses the kernel gradient to distribute the particle in two-dimensions such the simulation starts smoothly. Xiao et al. [6] proposes an algorithm to divide the 2D domain of interest into square shaped sub-domains. The sub-domains having area equal to the desired area (Δx^2) are directly converted to particles. Other particles near the boundary are given partial mass iteratively. Domínguez et al. [7] constructs geometries by clipping the grid with the boundary of the geometry, and this necessitates using a much higher resolution to capture the features better. None of these approaches consider three-dimensional geometries. Akinici et al. [4] propose a scheme to place particles over triangles of length greater then the particle spacing. This approach provides a good density distribution and has been employed to simulate flow for graphics applications in three dimensions.

It is important to note that the following features are desirable for an initial distribution of particles in the context of a fluid flow around a complex solid body:

- The particles defining the solid should capture the boundary surface accurately and not introduce artifacts due to the underlying structure of the discretization. As an example, a grid of points will never be able to conform to a curved boundary surface and introduces an artificial stair-case structure in the boundary.
- Boundary conditions are often set by using ghost particles inside the boundary and these particles too should be uniformly distributed.
- The initial distribution of fluid must conform to the contours of the body surface. This ensures that there are no artificial gaps or incorrect density variations when the simulation starts.
- The density of the resulting particle distribution should be as uniform as possible in both the fluid and solid domains.

In this paper, we propose a novel approach to construct two and three-dimensional geometries, at a given resolution, keeping the features of the geometry as detailed possible. The resulting particle distributions ensure an

accurate boundary, uniform density of particles in the interior of the solid, and in the fluid. It satisfies all the requirements listed above. The results presented in this paper show that these features are necessary in order to capture the forces on a body accurately.

We use the kernel gradient to move the particles as proposed by Colagrossi et al. [5] along with a strong repulsion force in order to resist particle clustering. The particles on the boundary are allowed to move over the surface only. The surface particles offer larger repulsion to each other so that they make themselves uniform over the boundary. Particles that are not on the boundary, are allowed to move in and out of the boundary surface. Due to the addition of the repulsive force the particles tend to equilibrate at unstable equilibrium configurations. In order to get rid of these, we introduce a simple agitation of the particles. Eventually these agitations are removed. It is important to note that the proposed algorithm can be applied in the context of any general purpose SPH framework. This makes the approach relatively easy to integrate into SPH codes. The present implementation uses the open source PySPH framework[8, 9].

It is important to capture the exact location of the boundary. This is especially so when we are interested in computing the forces on the body accurately. For example, consider the simple case of a two-dimensional circular disk of radius, R with its center at the origin. Should a solid particle be placed all along the circumference of the circle with radius R ? If the size of (or spacing between) the particle is of the order of Δx . Then clearly the true surface of the solid would extend to a radius greater than R .

Marrone et al. [10] propose a mirroring technique to implement solid boundary conditions where the interface particles are placed $\Delta x/2$ inside the true boundary of the interface, where Δx is the particle spacing. There are various methods proposed in literature for the implementation of solid boundary condition [11, 12, 13, 14]. The placement of the boundary depends upon the method used for solid boundary implementation. In this paper, we use the solid wall boundary condition proposed by Adami et al. [14]. In order to accurately capture no-slip at the boundary, we require to place the particle inside by $\Delta x/2$. Our proposed algorithm is able to displace the boundary surface particles by any desired amount as per the requirements.

The paper is divided into three sections. The next section describes the proposed particle packing algorithm. In section 3, we simulate a variety of problems using the proposed algorithm. In the interest of reproducibility, we make our implementation open source and all our results fully reproducible.

2. The Particle Packing Algorithm

Particle packing in and around a solid object is important if the forces are to be captured accurately. The particles must not only capture the shape of the boundary but should also have a uniform number density. In this section we discuss the proposed algorithm in detail.

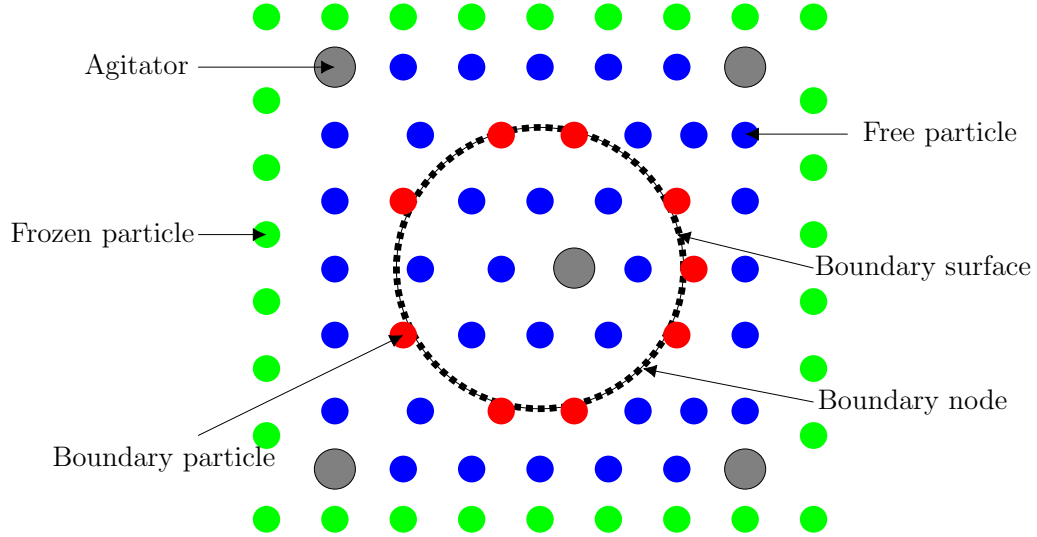


Figure 1: Schematic of the initial distribution of particles.

In Fig. 1, we show a schematic for an initial particle arrangement where the geometry in question is a circular cylinder. Our goal is to pack the particles inside and outside the cylinder such that the density of the resulting particles is almost constant, while capturing the boundary. In order to do this, different kinds of particles are employed in the algorithm and these are described below,

- *Free particles*: These are initially distributed uniformly in either a rectangular or hexagonal-packed arrangement and are allowed to move anywhere in the domain.
- *Frozen particles*: They may be thought as a set of fixed particles which contain the free particles.
- *Boundary surface*: The surface of the geometry we intend to capture. It is represented by a set of fixed particles which do not influence any other particles. The boundary surface is defined using “geometry nodes”.

- *Geometry node*: These are particles that discretize the boundary surface, they also capture the local surface normals of the geometry.
- *Boundary particles*: The particles which are constrained to move along the surface of the geometry (i.e. along the boundary surface).
- *Agitator particles*: These particles produce motion in the system so as to redistribute the particles smoothly. They move with a fixed speed in a predetermined path as discussed in section 2.3.

Given this initial distribution of particles, the overall flow of the algorithm is shown in fig. 2.

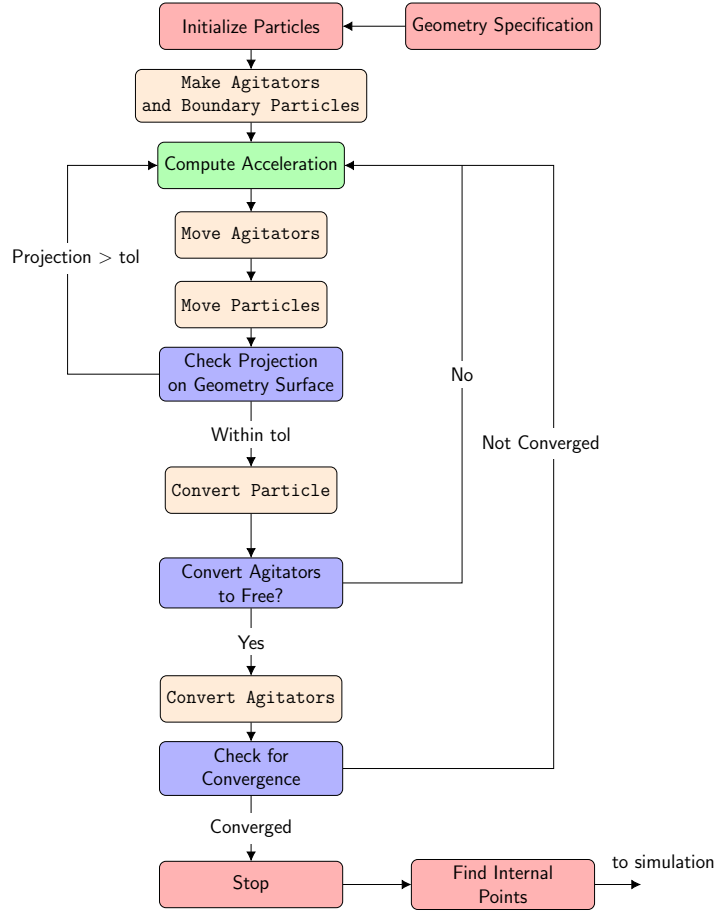


Figure 2: Flowchart of the particle packing algorithm.

The flowchart in fig. 2 is described below in a little more detail.

- The algorithm requires two inputs viz. the geometry information and the desired particle spacing. These are to be provided by the user.
- All the particles are initially placed on a regular hexagonal lattice. The particles that are closest to the boundary surface are converted to boundary particles as discussed in section 2.5. Some of the particles are converted to agitators, which impose motion on the free particles.
- The accelerations on the boundary and free particles (the green block in fig. 2) is computed using a number density gradient, and a repulsive force as discussed in section 2.1.
- The agitators are moved in a circular path in two dimensions and a spherical path in three dimensions.
- As the free particles move, if they are close enough to the geometry, they are converted to boundary particles. If the boundary particles are far away, they are converted to free particles. This is discussed in detail in section 2.5
- The boundary particles are constrained to move only along the geometry boundary as discussed in section 2.2.
- The agitators are converted to free particles only when there are no changes to the number of boundary particles for a large number of iterations as discussed in section 2.3.
- The algorithm stops when the density variation is less than a user-defined tolerance. We check for convergence only after the agitators are converted to free particles.

At the end of the iterations, the boundary and free particles inside and outside the geometry are packed as desired. The combination of the boundary and free particles may be placed anywhere in the main simulation in place of uniformly spaced points as shown in fig. 3. The particles inside the dashed box are the pre-processed particles divided into fluid and solid particles. We describe various aspects of the algorithm in the subsequent sections.

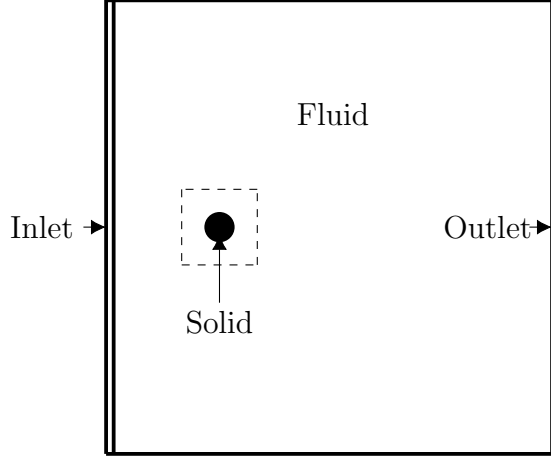


Figure 3: The preprocessed patch (dashed) placed in the appropriate location in a typical simulation.

2.1. Forces on Particles

In this section, we describe the forces acting on the particles. The two forces considered are due to a number density gradient, F_b and the second due to a repulsive force, F_k .

When particles are placed in a disordered fashion having mass, m and volume V_o , they exert a force, F_b on each other in order to reach an equilibrium position. This acceleration due to this force is given by

$$\frac{d\mathbf{u}}{dt}_b = -\frac{\nabla p_b}{\rho}, \quad (1)$$

where, p_b is the background pressure [5, 15]. In principle, the gradient of a constant pressure would be zero, however, when we employ an SPH discretization there is a spurious force due to the particle disorder. This spurious force is used to correct the particle position and obtain a uniform distribution of particles where the gradient goes to zero. Using SPH approximation, we discretize the above equation as

$$\frac{d\mathbf{u}_i}{dt}_b = \sum_j p_b \frac{V_i V_j}{m_i} \nabla W_{ij}, \quad (2)$$

where $V_i = \frac{m_i}{\rho_i}$ is the volume of the particles, where $\rho_i = \sum_j m_j W_{ij}$, $W_{ij} = W(|\mathbf{r}_i - \mathbf{r}_j|, h)$ is the kernel function chosen for the SPH discretization and h

is the support radius. The summation is over all the neighbors of particle i . In this paper, the quintic spline kernel is used given by,

$$W(q) = \begin{cases} \sigma [(3-q)^5 - 6(2-q)^5 + 15(1-q)^5], & \text{for } 0 \leq q \leq 1, \\ \sigma [(3-q)^5 - 6(2-q)^5], & \text{for } 1 < q \leq 2, \\ \sigma (3-q)^5, & \text{for } 2 < q \leq 3, \\ 0, & \text{for } q > 3, \end{cases} \quad (3)$$

where, $\sigma = 1/(120h^1)$, $7/(478\pi h^2)$, $3/(359\pi h^3)$ in one, two and three-dimensions respectively and $q = |\mathbf{r}|/h$. The selection of p_b is discussed in section 2.8. The number density gradient is a weak force. In the presence of agitators, the particles tend to clump and the displacements do not propagate to a large distance.

In order to resolve this problem, we add a repulsive force (RF), F_k similar to the Lennard Jones potential (LJP), given by

$$\frac{d\mathbf{u}}{dt}_{RF} = 12k \left(\frac{c^2}{r^3} - \frac{c}{r^2} \right), \quad (4)$$

where k , is a constant. We set the $c = 1.5\alpha\Delta x$, where α is the scaling factor. For free particles we set $\alpha = 1$ and for boundary particles we set $\alpha = 1.2$. In fig. 4, we show the comparison between the force due to LJP and the new suggested force. We can clearly see, that the LJ repulsion force increases rapidly compared to our suggested repulsion force. Moreover, unlike the LJP, the new force does not introduce inter-particle attraction.

Using SPH approximation, Equation. 4 can be written as

$$\frac{d\mathbf{u}_i}{dt}_{RF} = \sum_j \frac{12k\mathbf{x}_{ij}}{r_{ij}} \left(\frac{c^2}{r_{ij}^3} - \frac{c}{r_{ij}^2} \right). \quad (5)$$

As discussed in [5], we use a damping force, F_d to reduce the energy of the system. This is given by

$$\frac{d\mathbf{u}}{dt}_d = \zeta \mathbf{u}. \quad (6)$$

The value of the damping constant ζ is discussed in section 2.8. We discretize the eq. (6) as

$$\frac{d\mathbf{u}_i}{dt}_d = \zeta \mathbf{u}_i \quad (7)$$

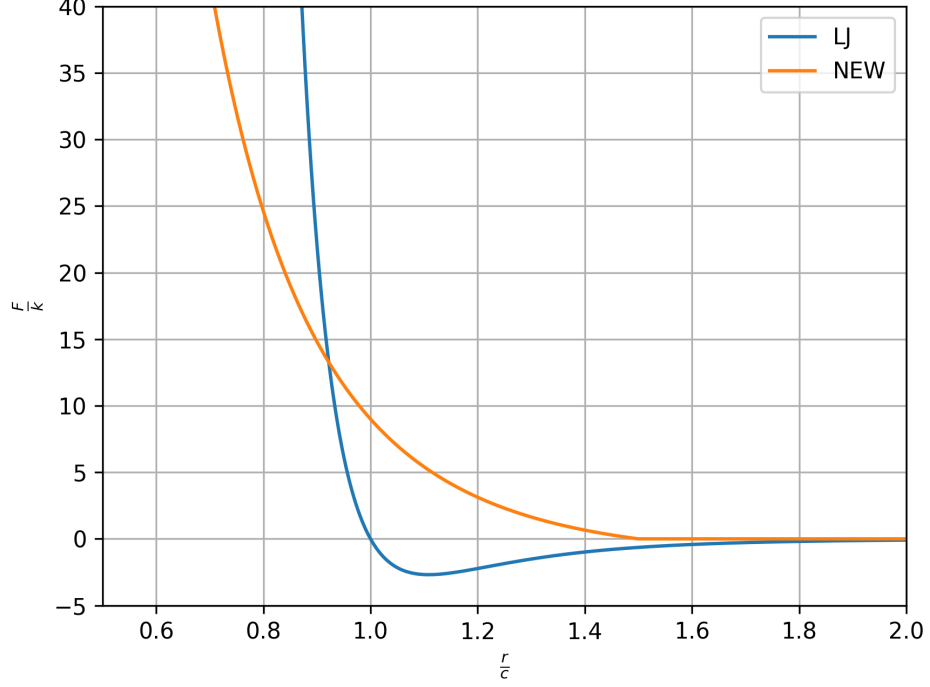


Figure 4: Force due to LJ potential and new suggested force as a function of distance, r .

where, v_i is the velocity of the i^{th} particle. Thus, the total force on the particles is given by

$$\frac{d\mathbf{u}}{dt} = -\frac{\nabla p_b}{\rho} + 12k \left(\frac{c^2}{r^3} - \frac{c}{r^2} \right) + \zeta \mathbf{u} \quad (8)$$

The above equation can be converted into SPH form using eqs. (2), (5) and (7). On evaluating the RHS using eq. (8) the velocities and new positions are calculated using Euler integration given by

$$\begin{aligned} u_i(t + \Delta t) &= u_i(t) + \Delta t \left(\frac{d\mathbf{u}}{dt} \right)_i \\ r_i(t + \Delta t) &= r_i(t) + \Delta t u(t + \Delta t) \end{aligned} \quad (9)$$

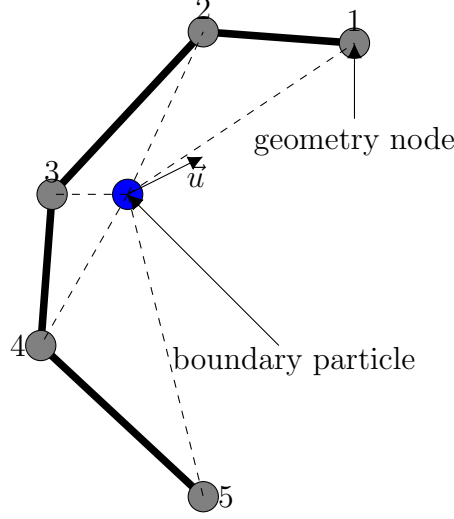


Figure 5: Motion of boundary particle along the geometry.

2.2. Motion of Boundary Particles

At $t = 0$ the free particles nearest to the body are converted to boundary particles. Motion of the boundary particles are restricted. We move the boundary particles along the boundary surface. In fig.5 we illustrate the motion of a boundary particle (in blue) along the geometry represented by nodes 1, 2, 3, 4 and 5. We first find the geometry node nearest to the boundary particles in the direction of the particle's velocity. Consider a boundary particle i , and a boundary node j , near i . The nearest node n_i is determined by

$$n_i = j \mid \min(r_{ij}) \text{ and } \mathbf{x}_{ij} \cdot \mathbf{u}_i < 0 \quad (10)$$

where, $\mathbf{x}_{ij} = \mathbf{x}_i - \mathbf{x}_j$, $r_{ij} = |\mathbf{x}_{ij}|$ and \mathbf{u}_i is the velocity of the boundary particle. Using the nearest node, n_i the direction of motion, $\hat{x}_n = -\hat{\mathbf{x}}_{in_i}$. Thus, the boundary particle position is updated using the following equation

$$\mathbf{x}_i = \mathbf{x}_i + (\mathbf{u}_i \cdot \hat{x}_n) \hat{x}_n. \quad (11)$$

2.3. Motion of Agitators

The agitators introduce a small amount of motion in their vicinity. Many agitators are distributed inside among the free particles in order to move the particles. The agitators are selected using a coarser grid over the free particles. The free particles overlapping agitators are removed from the domain.

The agitators are not placed near the boundary geometry to avoid excess motion near the boundary. The agitators are placed $2\Delta x$ distance away from the boundary surface. The motion of the agitator in two dimensions is given by

$$\begin{aligned} \mathbf{x} &= \mathbf{x}_{\mathbf{t}=\mathbf{0}} + \frac{\Delta x}{2} \cos(\omega t), \\ \mathbf{y} &= \mathbf{y}_{\mathbf{t}=\mathbf{0}} + \frac{\Delta x}{2} \sin(\omega t). \end{aligned} \tag{12}$$

Similarly, in three dimensions

$$\begin{aligned} \mathbf{x} &= \mathbf{x}_{\mathbf{t}=\mathbf{0}} + \frac{\Delta x}{2} \cos(0.5\omega t) \sin(\omega t), \\ \mathbf{y} &= \mathbf{y}_{\mathbf{t}=\mathbf{0}} + \frac{\Delta x}{2} \sin(0.5\omega t) \sin(\omega t), \\ \mathbf{z} &= \mathbf{z}_{\mathbf{t}=\mathbf{0}} + \frac{\Delta x}{2} \cos(\omega t) \end{aligned} \tag{13}$$

where, ω is the angular velocity by which agitators move in a circular and spherical paths in 2D and 3D domain respectively. The agitators move with constant angular velocity and are converted to free particles when the number of boundary particles do not change for 4000 iterations (this corresponds to 1 revolution of the agitator).

2.4. Initialization of particles

We first initialize the geometry surface and boundary particles. In a two-dimensional domain, a set of consecutive points are required to define the boundary surface. The geometry nodes are identified as the mid-points of the consecutive points that define the surface. The outward normals n_x, n_y are calculated using

$$\begin{aligned} n_x &= \frac{y_{i+1} - y_i}{d} \\ n_y &= -\frac{x_{i+1} - x_i}{d} \end{aligned} \tag{14}$$

for the i^{th} point, where d is the length of the segment.

For a three-dimensional case, a stereolithography (STL) file with outward normals is necessary. The boundary geometry is shifted $\Delta x/2$ distance inside the actual boundary to correctly implement solid boundary condition [10].

In order to move the boundary inwards the following translation is done to each boundary node for 3D/2D

$$\vec{x} = \vec{x} - \frac{\Delta x}{2} \hat{n}, \quad (15)$$

where, \vec{x} is the position and \hat{n} is the unit normal. In special cases where we have sharp changes in the features of the geometry as in an airfoil trailing edge, when the points are moved inside, the boundary surface may self-intersect. In those cases, one has to carefully remove some particles manually from the boundary geometry.

2.5. Converting boundary and free particles

Initially the boundary particles are unlikely to conform to the boundary surface. The boundary and free particles move and as they move, they may be inter-converted.

Consider a free particle that is close to the boundary surface. We find the nearest geometry node and find the distance to this node along the normal. If the projected distance is less than $\Delta x/10$ and has a velocity less than $u_a = \omega \Delta x/2$ (the velocity of the agitator), where ω is the angular velocity of the agitator, it is converted into a boundary particle. The velocity criteria is imposed in order to not convert any fast moving particles. Similarly, if the projected distance of a boundary particle to its nearest geometry node is greater than $\Delta x/4$, it is converted into a free particle.

The particle conversion is not performed every time step but once every N_d iterations in order to allow particles to move a sufficient distance, given by

$$N_d = \frac{0.1 \Delta x}{u_a \Delta t_{max}} \quad (16)$$

where $\Delta t_{max} = h^2/\zeta \approx 10^{-4} s$ for all our simulation.

2.6. Convergence Criteria

In order to stop the simulation, the L_∞ norm of density fluctuations is set as the convergence criteria. The particle masses are equal and hence when the distribution of particles is uniform, the density must also be uniform. The simulation stops when

$$|L_\infty(|\rho_i^{t+T} - \rho_o|) - L_\infty(|\rho_i^t - \rho_o|)| < 10^{-3}. \quad (17)$$

where, t is the time, and T is set such that the agitator completes one revolution. For all our simulations $\rho_o = \sum_j m_j W_{oj}$ at $t = 0$ when the particles are uniformly distributed.

2.7. Separating interior and exterior particles

At the end of the simulation, both interior (particles inside the boundary surface) and exterior particles (particles outside the boundary surface) are uniformly distributed. The interior particles along with the boundary particles are extracted and used as solid particles, while the rest of the particles are used as fluid particles. The detection of the interior particles may be performed with well known algorithms which we outline below.

Figure 6 depicts a two-dimensional boundary surface as a dashed line and free particles in blue all over the domain both inside and outside the geometry with boundary particles shown in red.

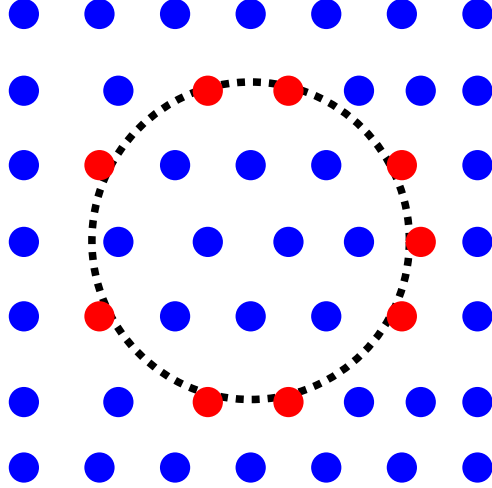


Figure 6: The boundary in red and all the particles shown in blue dots.

We use the well known ‘signed angle method’ [16] in order to determine the points inside the boundary. The angle subtended by the vector joining the point to two consecutive boundary points is evaluated, such that the angle is of positive sign when moving in the direction of the curve. For each pair of consecutive points, we get an angle θ_i between the dashed/dotted lines. The motion in clockwise direction will give a negative angle and vice-versa. The point is inside the domain if $\sum \theta_i > \pi$.

In case of a three-dimensional geometry, we use well known ‘ray shooting method’ [16]. A ray is passed in the positive x direction. If the ray intersects the geometry an odd number of times then the point is an internal point otherwise it is outside.

2.8. Determining the constants and time-step

In the proposed algorithm, we encounter many constant which may affect the simulation in different ways. In order to have a consistent behavior we heuristically fix the values of parameters like p_b, ζ, k , and ω . We performed some numerical experiments to determine a suitable combination of parameters such that the spring and number density forces are of similar magnitude. To do this we perturb a single particle by $\Delta x/4$ in a 2D and 3D lattice and found the following relation to produce roughly the same magnitude of forces,

$$p_b = 2000(d - 1)k, \quad (18)$$

where k is the repulsion constant and d is the dimension of the problem. Given this, we choose $k = 1$. The damping, ζ is linked with p_b similar to [5] and is given by

$$\zeta = 5 \times 10^{-3} \frac{\sqrt{p_b}}{\Delta x}. \quad (19)$$

Furthermore, the agitator frequency, ω is set to $2\pi/\tau$ where $\tau = 0.2$ such that the agitator does not move too fast but not too slow so as to increase the simulation time.

The time-step, Δt used in the simulation is adaptive and is calculated after evaluating the acceleration of every particle and given by,

$$\Delta t_{adapt} = \min \left(\frac{0.01\Delta x}{|\mathbf{u}_i + \mathbf{a}_i\Delta t|} \right) \quad (20)$$

where \mathbf{u}_i and \mathbf{a}_i are the velocity and acceleration of a particle at the time t .

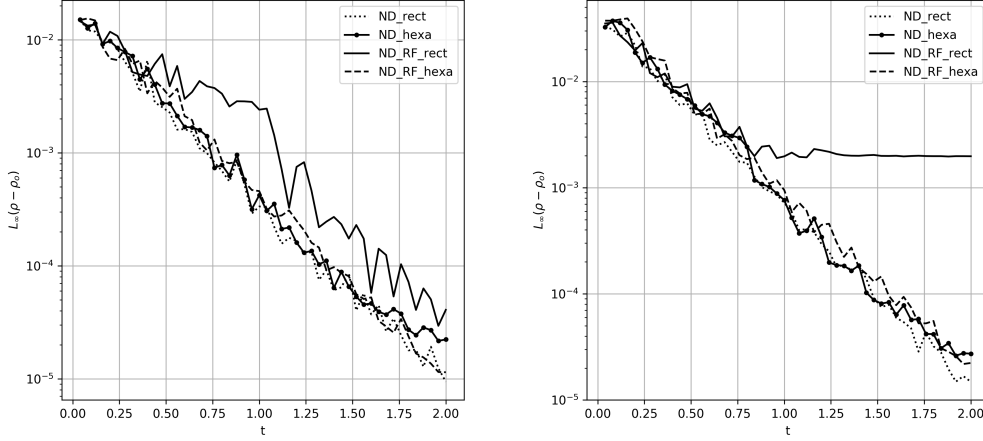
The proposed algorithm is implemented in the open-source SPH framework, PySPH [17, 9, 8]. Our implementation is also open source and freely available with this manuscript at https://gitlab.com/pypr/sph_geom. All the results shown in the next section are fully reproducible using a simple automation framework [18].

3. Results and discussion

In this section we compare the new algorithm with traditional approaches used in the SPH literature. One common way of defining the geometry in SPH is to arrange the particles in a rectangular grid and select the points that only lie within the boundary surface [7]. We call this *clipping*. Another method in two dimensions is to use a triangulation of the geometry and then convert the triangles to particles located at the centroid of each triangle with volume equal to that of the corresponding triangle area. This volume is multiplied by the required density and set as the mass of the solid particle. The triangulation is usually performed so as to ensure a uniform size of particles and stored in an STL file. We call this approach, *triangulation*.

In this section, we compare the result for geometries made using these methods and the proposed method. We show that the proposed method captures the geometry more accurately. We show that this results in an improvement in results even at lower resolution. We demonstrate that the boundary conditions are imposed accurately with the method.

3.1. Packing stability in 2D



(a) With finite perturbation.

(b) With agitation.

Figure 7: Density convergence in two-dimensions.

We assess the stability of the scheme in two dimensions as done by Colagrossi et al. [5]. Particles are initially packed using a rectangular or hexagonal distribution. A perturbation is introduced and the stability of the algorithm and distribution is assessed for various cases. The following are the distinct cases:

- hexagonal packing with number density (ND) gradient.
- hexagonal packing with ND + repulsion force (RF).
- rectangular packing with ND gradient.
- rectangular packing with ND + RF.

We consider a 20×20 grid of particles that is periodic in both x and y . The particles are spaced uniformly with $\Delta x = 0.05$ and $h/\Delta x = 1.2$. We consider the reduced damping constant equal to 10% of the value described in section 2.8. A middle node is perturbed with a displacement of $\Delta x/4$. No agitators are used in these cases. Fig. 7a shows the $L_\infty(\rho - \rho_o)$ of the system with time. Clearly, all the cases show a similar convergence rate. The hexagonal configuration with ND+RF is smoother than a rectangular arrangement.

We next test the stability of the packing and the different kinds of forces in the presence of agitators. An agitator is placed at the center replacing a free particle. It remains active until $t = 0.1s$ and is then converted into a free particle. In Fig. 7b, we plot $L_\infty(\rho - \rho_o)$ of the system with time. It is evident from the plot that in presence of the repulsive force the rectangular configuration attains an intermediate arrangement. All the other combinations show similar convergence rates. This suggests that the hexagonal packing arrangements are more stable.

3.2. Flow past a circular cylinder

The flow of an incompressible fluid past a cylinder is a well known benchmark problem. In this test case we compare the flow over the cylinder constructed using the proposed approach with that using triangulation and clipping. In this simulation, we consider a cylinder of diameter $D = 2m$. The size of the domain is $15D \times 15D$, which is sufficient in order to avoid the effect of the wall. The cylinder is kept at $5D$ distance from the inlet at the center. The particle spacing $\Delta x = 0.1$ with $h/\Delta x = 1.2$. We use a fluid with density $\rho = 1000kg/m^3$ and dynamic viscosity $\nu = 0.01$. The inlet, outlet

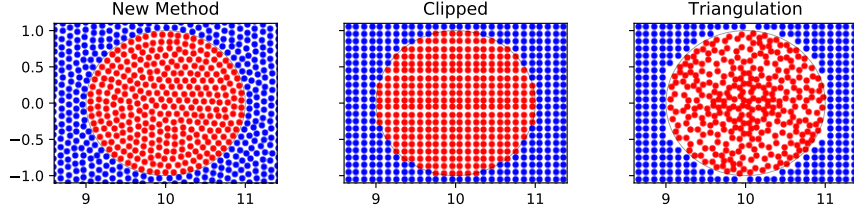


Figure 8: The particle distribution for the flow past circular cylinder produced using the different methods.

and wall are made using 6 layers of particles in order to provide full kernel support for the fluid particles. Inlet particles are initialized with velocity $(1.0, 0.0, 0.0)$. The inlet and outlet boundary are implemented using method proposed by Negi et al. [19]. In fig. 8, we compare the geometry made from different methods. It can be seen that the geometry made from proposed method captures the boundary well, whereas the standard method results in a zig-zag pattern. The geometry made using a triangulation results in an uneven distribution of particles.

We simulate the flow past a cylinder using the different geometries for the conditions mentioned above. In Fig. 9, we plot the velocity snapshot at $t = 120s$ for all the geometries. The pre-processed geometry smoothly allows particles to flow over the surface compared to the other cases where the particles appear to be penetrating the boundary. The forces on the cylinder are calculated using the method given in [19]. In Fig. 10a, we plot the c_d and c_l for all the geometries. The new method shows a smoother variation compared to that of the geometry made using clipping. In case of the geometry generated from the triangulation, a significant delay in shedding can be observed. However, the values of c_d and maximum c_l are close to 1.46 and 0.693 respectively for all the geometries and this is the same as provided in literature [20, 19].

As mentioned earlier, we place the particles $\Delta x/2$ inside the actual boundary surface. To study how well this satisfies the no-slip boundary condition, we consider the solution at a time of 150s. In fig. 10b, we plot the velocity at the cylinder surface, $r = 1$, versus the angular position θ . This velocity is computed by using an SPH interpolation. It is clear that the new method has lower variations at the cylinder surface compared to the other methods.

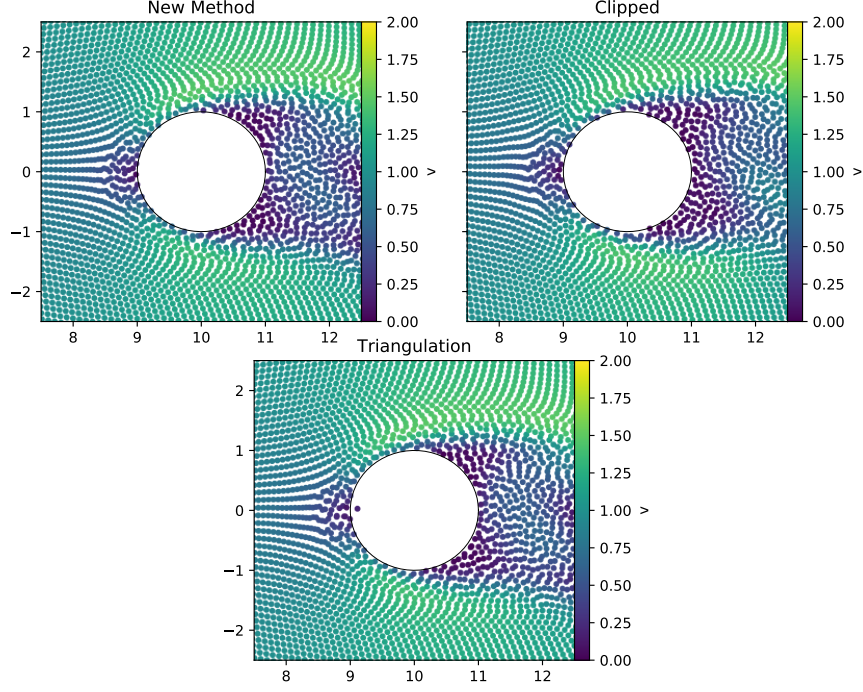
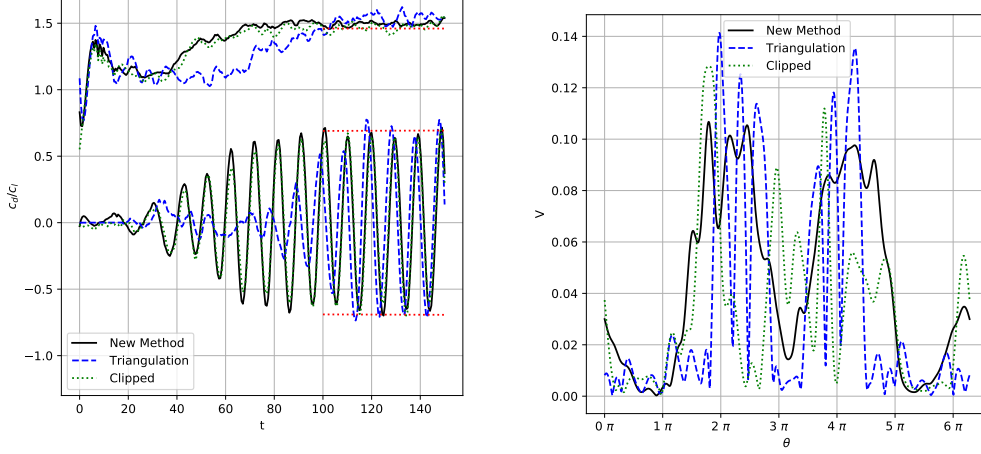


Figure 9: Velocity plots for the flow past a cylinder for $Re = 200$ at $t = 120s$.

3.3. Taylor-Couette flow

We compare the Taylor-Couette flow for the geometry made using clipping and the proposed method. We consider two concentric cylinders with outer cylinder of radius, $b = 0.5m$ and inner with radius, $a = 0.25m$. The inner cylinder is rotating with an angular velocity, $\Omega_a = 1rad/s$, whereas the outer cylinder is stationary i.e $\Omega_b = 0.0rad/s$. Since we pull the surface $\Delta x/2$ inside, in order to impose correct velocity we rotate the inner cylinder with $\Omega'_a = \Omega_a a / (a - 0.5\Delta x)$. The exact solution for the azimuth velocity, u_ϕ is given by

$$u_\phi = C_1 r + \frac{C_2}{r} \quad (21)$$



(a) c_d and c_l plot for cylinder where Dashed red line shows the expected value.

(b) Velocity along the surface of the cylinder with the different geometries.

Figure 10: Drag and lift coefficient and surface velocity distribution for flow past a circular cylinder.

where,

$$C_1 = \frac{\Omega_b b^2 - \Omega_a a^2}{b^2 - a^2} \text{ and } C_2 = \frac{(\Omega_b - \Omega_a) a^2 b^2}{b^2 - a^2}$$

We simulate the problem for a time of 60s (corresponding to around 10 revolutions), we use a kinematic viscosity of $0.2m^2/s$. In fig. 11 we show the L_2 norm of $(u - u_\phi)$ where u is the value from the numerical simulation. The results are shown for the last 10s of the simulation where the values have converged. Clearly, the new method shows a lower L_2 norm. In the case of the clipped geometry, we can see periodic increases in the error which occurs due to the non-smooth surface. Our proposed method results in reduction of noise, as well as accurate implementation of solid BC.

3.4. Flow Past 2D Airfoil

We consider the flow past a symmetric airfoil, NACA0015 for similar flow conditions as in the flow past a circular cylinder. In fig. 12a, we show the distribution of particles created by the proposed algorithm and compare

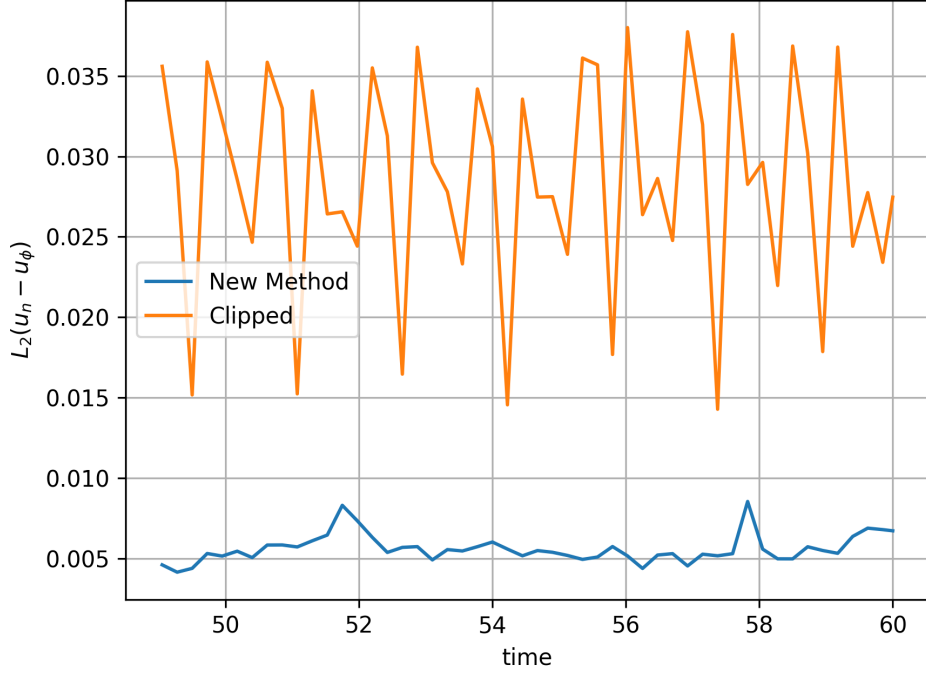


Figure 11: Comparison of $L_2(u - u_\phi)$ with time.

it with the other approaches. It can be seen that the proposed algorithm captures the curvature of the surface well. The standard method results in a stepped surface and the triangulation based approach produce an uneven distribution of particles.

We simulate the flow past this airfoil with a free-stream at $1m/s$ and zero angle of attack. Figure 12b shows the distribution of particles and the colors indicate the velocity magnitude as simulated using the different methods at $t = 46s$. The stepped arrangement of particles when using clipping introduces some artifacts while the triangulation introduces an artificial force pushing back on the particles. Clearly the new method produces much better results.

3.5. Arbitrary Shaped Geometry

In this example, we apply the proposed algorithm on an arbitrary shaped body. We show the packing at different particle spacings in fig. 13. The

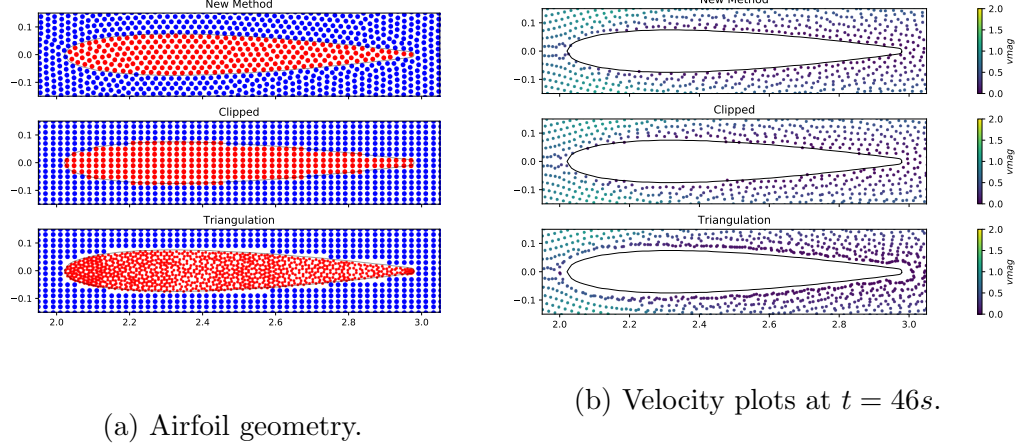


Figure 12: The initial particle distribution and the particle velocity plots during the fluid simulation for the different packing methods.

particle spacings chosen are 0.05, 0.075, and 0.1. We place the particles at $\Delta x/2$ distance away from the boundary. We can clearly see that the density distribution is close to the desired value of 1.0. The particles conform to the body surface. This shows that the proposed algorithm is applicable to complex two-dimensional geometries.

3.6. Stability in 3D

Similar to the stability test performed for a two-dimensional lattice, we perform a stability analysis on a three-dimensional lattice. We consider a $4 \times 4 \times 4$ lattice of particles, with spacing $\Delta x = 0.1$. The grid is surrounded by 5 layers of frozen particles in order to provide kernel support. In the fig. 14a, we observe the rectangular lattice not converging to it's original position. However adding a repulsive force clearly helps to attain a better configuration. In fig. 14b, we can clearly see the addition of agitator do not decrease the initial rate of convergence. At $t = 0.1s$, we convert the agitators to free particles. The rectangular configuration approaches a different equilibrium position where the density variations are larger. This test-case shows that the hexagonal packing is a stable configuration in three dimensions as well. Hence, for all of our test cases we use hexagonal packing with ND+RF gradient along with damping.

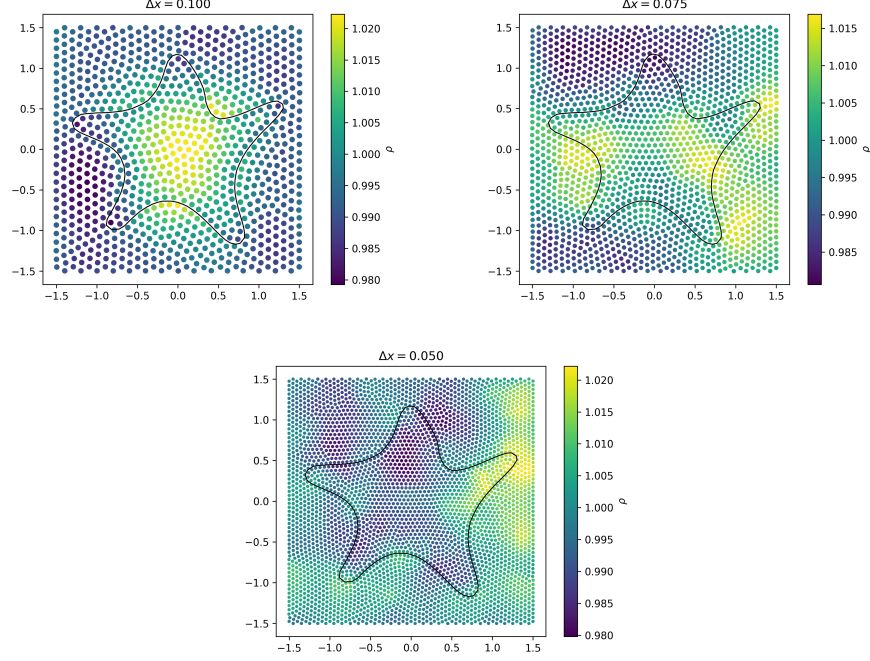
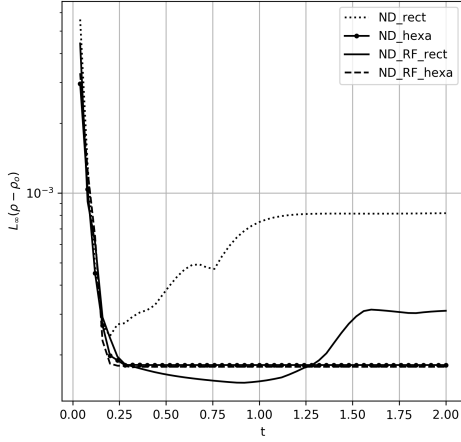


Figure 13: Particle plots at different resolutions for arbitrary shaped object.

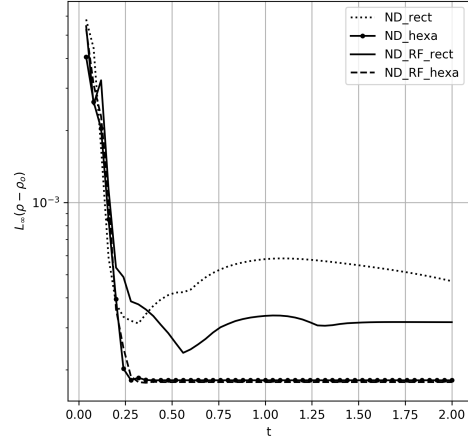
3.7. Flow past a sphere

We next simulate the flow past a sphere of diameter, $D = 2m$. The Reynolds number of the flow is 20. The flow conditions are similar to those used in the flow past cylinder. Since the Reynolds number is low, we consider a smaller domain of size $5D \times 2D \times 2D$. In Fig. 15, we show the geometry made using the proposed method and with clipping. We scale the original boundary by 0.95 to visualize the particles on the surface. Clearly, the geometry constructed using the proposed method show a uniform distribution on the geometry. The geometry made using clipping has an uneven particle arrangement near the surface.

In fig. 17, we plot the velocity magnitude of a slice through the particle field with the velocity magnitude interpolated on the surface. We can see that, the velocity plot for the flow past new geometry has a shift in the legend where it show a lower velocity near the sphere. Thus the geometry from the proposed method improves the quality of no-slip BC implementation. We also compare the drag from the clipped geometry with the one made using

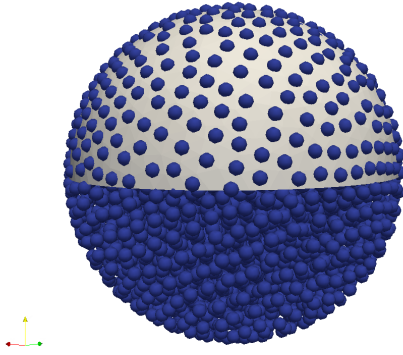


(a) With finite perturbation.

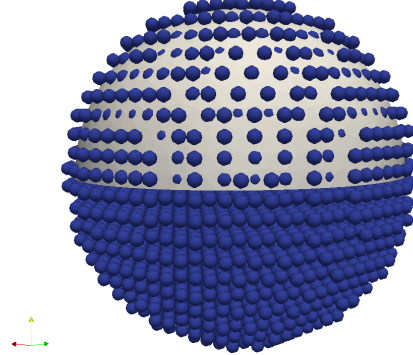


(b) With agitation.

Figure 14: The evolution of the L_∞ norm of the density of the particles in time.



(a) New Method.



(b) Clipped.

Figure 15: Particle distribution for a sphere with the different methods.

the proposed algorithm. In Fig. 16, we show the drag coefficient, c_d for both the geometries. It is evident from the plot that the new geometry produces a result close to the experimental value of 2.925 [21].

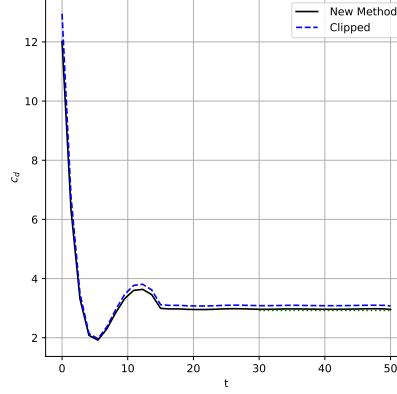


Figure 16: c_d for flow past sphere at $Re=20$ with dashed green shows the expected value.

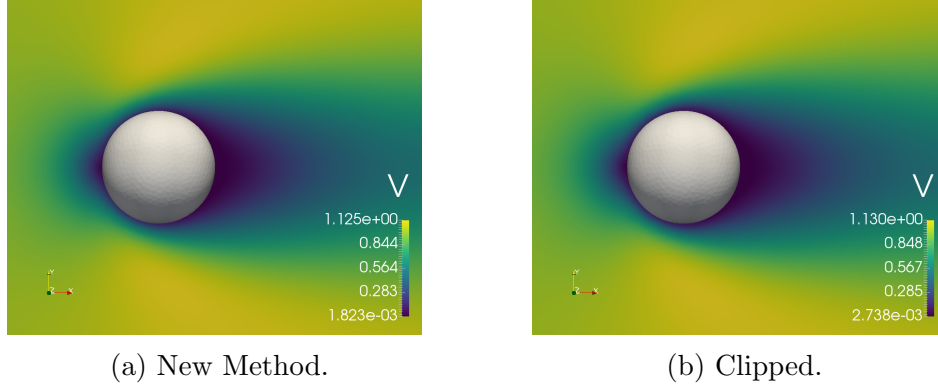


Figure 17: velocity for flow past sphere for $Re=20$ at $t = 50s$.

3.8. Packing particles on the Stanford Bunny

We apply the proposed algorithm to the ‘Stanford Bunny’. The original geometry available has a small size of the order of 10^{-2} , we scale it by a factor of 10. The geometry surface required must have outward normals, and we correct mesh using a mesh manipulation tool. The particle spacing is 0.02. In this case, we are only interested in showing how well we capture the geometry so we do not move the surface particles into the geometry. In fig. 18, we show the particle distribution over the surface of the bunny. Clearly the results from the geometry made from proposed method has uniform particles. The method using clipping does not capture the tail and ears accurately. The

results show the applicability of the proposed algorithm to arbitrary shaped 3D objects. After pre-processing the 3D object can be placed anywhere in the domain, with the surrounding particles.

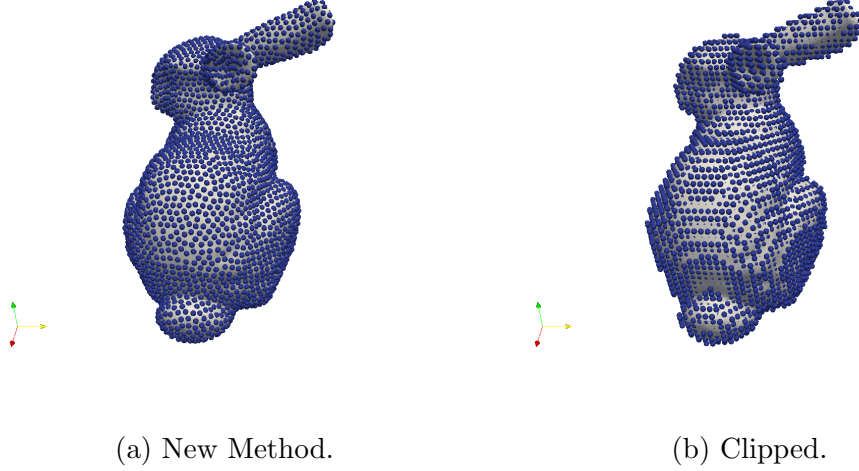


Figure 18: Stanford Bunny Particle distribution of particles on the surface.

4. Conclusions

This paper proposes an improved particle packing algorithm for the simulation of flows involving complex geometries in two and three dimensions. The method produces homogeneous particle distributions inside and outside the boundary surface while capturing the boundary surfaces accurately. The algorithm employs a number density gradient and damping as suggested by Colagrossi et al. [5] but adds a repulsive force along with agitators to generate smooth particle distributions. Several benchmark cases are shown which highlight the accuracy of the proposed algorithm in two and three dimensions. The algorithm may be applied as a pre-processing step before a mesh-free particle simulation. This allows us to implement solid boundary conditions accurately.

References

References

1. Gingold, R.A., Monaghan, J.J.. Smoothed particle hydrodynamics: Theory and application to non-spherical stars. *Monthly Notices of the Royal Astronomical Society* 1977;181:375–389.
2. Lucy, L.B.. A numerical approach to testing the fission hypothesis. *The Astronomical Journal* 1977;82(12):1013–1024.
3. Morris, J.P., Fox, P.J., Zhu, Y.. Modeling low reynolds number incompressible flows using SPH. *Journal of Computational Physics* 1997;136(1):214–226. doi:<http://dx.doi.org/10.1006/jcph.1997.5776>.
4. Akinci, N., Cornelis, J., Akinci, G., Teschner, M.. Coupling elastic solids with smoothed particle hydrodynamics fluids. *Computer Animation and Virtual Worlds* 2013;24(3-4):195–203.
5. Colagrossi, A., Bouscasse, B., Antuono, M., Marrone, S.. Particle packing algorithm for SPH schemes. *Computer Physics Communications* 2012;183(8):1641–1653.
6. Xiao, Y., Dong, H., Zhan, H., Gu, Y.. A new particle generation method for arbitrary 2D geometries in SPH modeling. *International Journal of Computational Methods* 2017;14(03):1750023.
7. Domínguez, J., Crespo, A., Barreiro, A., Gómez-Gesteira, M., Mayrhofer, A.. Development of a new pre-processing tool for sph models with complex geometries. In: *6th International SPHERIC workshop*. 2011:117–124.
8. Ramachandran, P.. PySPH: a reproducible and high-performance framework for smoothed particle hydrodynamics. In: Benthall, S., Rostrup, S., eds. *Proceedings of the 15th Python in Science Conference*. 2016:127 – 135.
9. Ramachandran, P., Puri, K., Bhosale, A., Adep, D., Muta, A., Negi, P., Govind, R., Sanka, S., Pandey, P., Kaushik, C., Kumar, A., Sen, A., Kaushik, R., Patil, M., Tavker, D., Menon,

- D., Kurapati, V., Sebastian, A.S., Dutt, A., Agarwal, A.. PySPH: a Python-based framework for smoothed particle hydrodynamics. *arXiv preprint arXiv:1909.04504* 2019;URL: <https://arxiv.org/abs/1909.04504>.
10. Marrone, S., Antuono, M., Colagrossi, A., Colicchio, G., Le Touzé, D., Graziani, G.. δ -SPH model for simulating violent impact flows. *Computer Methods in Applied Mechanics and Engineering* 2011;200:1526–1542. doi:10.1016/j.cma.2010.12.016.
 11. Wang, L., Ge, W., Li, J.. A new wall boundary condition in particle methods. *Computer Physics Communications* 2006;174(5):386 – 390. URL: <http://www.sciencedirect.com/science/article/pii/S0010465505005862>. doi:<https://doi.org/10.1016/j.cpc.2005.11.004>.
 12. Chen, Y.s., Zheng, X., Jin, S.q., Duan, W.y.. A corrected solid boundary treatment method for smoothed particle hydrodynamics. *China Ocean Engineering* 2017;31(2):238–247. doi:10.1007/s13344-017-0028-z.
 13. Bouscasse, B., Colagrossi, A., Marrone, S., Antuono, M.. Non-linear water wave interaction with floating bodies in SPH. *Journal of Fluids and Structures* 2013;42:112 – 129. URL: <http://www.sciencedirect.com/science/article/pii/S0889974613001266>. doi:<https://doi.org/10.1016/j.jfluidstructs.2013.05.010>.
 14. Adami, S., Hu, X., Adams, N.. A generalized wall boundary condition for smoothed particle hydrodynamics. *Journal of Computational Physics* 2012;231(21):7057–7075. URL: <http://linkinghub.elsevier.com/retrieve/pii/S002199911200229X>. doi:10.1016/j.jcp.2012.05.005.
 15. Adami, S., Hu, X., Adams, N.. A transport-velocity formulation for smoothed particle hydrodynamics. *Journal of Computational Physics* 2013;241:292–307. URL: <http://linkinghub.elsevier.com/retrieve/pii/S002199911300096X>. doi:10.1016/j.jcp.2013.01.043.

16. Laszlo, M.J.. Computational Geometry and Computer Graphics in C++. Upper Saddle River, NJ, USA: Prentice-Hall, Inc.; 1995. ISBN 0-13-290842-5.
17. Ramachandran, P., Puri, K., et al. PySPH: a python-based SPH framework. 2010-. URL: <http://pypi.python.org/pypi/PySPH/>.
18. Ramachandran, P.. automan: A python-based automation framework for numerical computing. *Computing in Science & Engineering* 2018;20(5):81–97. URL: doi.ieeecomputersociety.org/10.1109/MCSE.2018.05329818. doi:10.1109/MCSE.2018.05329818.
19. Negi, P., Ramachandran, P., Haftu, A.. An improved non-reflecting outlet boundary condition for weakly-compressible sph. *arXiv preprint arXiv:190704034* 2019;URL: <https://arxiv.org/abs/1907.04034>.
20. Tafuni, A., Domínguez, J., Vacondio, R., Crespo, A.J.C.. A versatile algorithm for the treatment of of open boundary conditions in smoothed particle hydrodynamics GPU models. *Computer methods in applied mechanical engineering* 2018;342:604–624. doi:10.1016/j.cma.2018.08.004.
21. Roos, F.W., Willmarth, W.W.. Some experimental results on sphere and disk drag. *AIAA journal* 1971;9(2):285–291.